Investigation of Hydrogen Storage Capabilities of ZnO-Based Nanostructures

Mashkoor Ahmad,[†] Rafi-ud-Din,[‡] Caofeng Pan,[†] and Jing Zhu*,[†]

Beijing National Center for Electron Microscopy, The State Key Laboratory of New Ceramics and Fine Processing, Laboratory of Advanced Material, Department of Material Science and Engineering, Tsinghua University, Beijing 100084, China, and State Key Laboratory for Advanced Metals and Materials, School of Materials Science and Engineering, University of Science & Technology, Beijing 100083, China

Received: November 19, 2009; Revised Manuscript Received: January 11, 2010

Hydrogen storage capabilities of controlled synthesized ZnO-based nanostructures have been investigated. The microscopic results reveal that the products consist of hollow ZnO microspheres composed of nanowires, hollow Sb-doped nanospheres, and Al-doped nanobelts. Energy dispersive spectroscopy (EDS) and X-ray photoelectron spectroscopy (XPS) give evidence that Sb and Al dopants are successfully substituted into nanospheres and nanobelts, respectively. The photoluminescence (PL) spectra exhibit a strong green emission band due to defects in nanostructures which lead to a significant role in the hydrogen storage applications. The hydrogen storage characteristics prove that the defects in nanostructures are responsible for higher hydrogen absorption. Among the nanostructures the maximum hydrogen storage capacity of about 2.94 wt % is achieved under the pressure of 5 MPa for Al-doped ZnO nanobelts, and about 81.6% of the stored hydrogen can be released under ambient pressure at 373 K. The highly reversible absorption/desorption reactions exhibit that Al-doped nanobelts are promising material for hydrogen storage.

I. Introduction

ZnO is one of the most promising material because of a direct wide band gap $E_g = 3.37$ eV and large exciting binding energy (60 meV) at room temperature. It has been found useful in many applications such as opt-electronic devices.[1] Recently, intensive research has been focused on fabricating ZnO nanostructures such as nanospheres, nanowires (NWs), and nanobelts due to their shaped induced novel properties and potential applications.[2,3] Hydrogen is considered as an efficient and clean fuel for the future due to its abundance, easy synthesis, and nonpolluting nature.[4] Hydrogen storage in nanostructure is critical to the development of future transportation technologies, such as H_2 fuel cell vehicles.[5] In recent years, many attempts have been made to improve the hydrogen storage properties such as doping with selective elements, modifying surface properties, and employing novel preparation techniques.[6] Among them doping with selective elements[7] offers an effective approach to improve the properties, which is crucial for their practical applications.

Recently, carbon nanotubes as well as metal hydrides have attracted extensive attention as promising hydrogen storage materials.[8–12] Additionally, nanostructures BN,[13] TiS_2,[14] WCNTs,[15] and SiCNT[16] have been investigated as possible hydrogen storage materials.[17] As a wide band gap semiconductor, ZnO has also been investigated as a hydrogen storage material.[18,19] However, due to the increasing needs of ZnO for the applications in energy storage materials, some attempts are made to further improve the hydrogen storage properties of ZnO nanostructures by the addition of metals, e.g., Sb and Al. The nanostructures such as hollow ZnO nanospheres composed of NWs, Sb-doped ZnO nanospheres, and Al-doped ZnO nanobelts are synthesized via a controllable thermal evaporation method. The hydrogen absorption/desorption capabilities of these nanostructures have been investigated by pressure composition and temperature (PCT) apparatus.

II. Experimental Section

Controllable syntheses of ZnO nanostructures were carried out in a horizontal quartz tube furnace, where the temperature, pressure, and flow rates of working gases are well controlled.

1. Synthesis of ZnO Microspheres. ZnO microspheres with NWs grown on the outer surfaces were synthesized by a two-step thermal process approach. In the synthesis steps, high-purity metallic Zn powder (99.9%) was first dispersed in ethanol (5% by weight). Two drops of the dispersant were deposited on the cleaned Si substrate and subsequently dried in air at room temperature for 5 h. As a result a thin layer of Zn particles was formed on the substrate. The predeposited Zn particles act as temporary templates to form ZnO microspheres, while a mixture (Zn + ZnO) powder (2:1 in atomic ratio) was placed at the center of a quartz tube for growing ZnO NWs on the outer surfaces of microspheres. The substrate with a thin layer of Zn particles was located downstream 10 mm away from the source material. Mixed gas (90% Ar, 10% O_2) flows through the quartz tube at a rate of 200 sccm. The furnace temperature was increased to a designated temperature of 750 °C at a speed of 10 deg min^{-1}. The mixed gas was maintained throughout the whole reaction process for 3 h. The synthetic product was cooled to room temperature with the mixed gas flow.

2. Sb-Doped ZnO Hollow Nanospheres. Sb-doped ZnO nanospheres were also synthesized via a two-step thermal process, where predeposited Zn particles on Si substrate act as a temporary template, while mixed powder Zn + Sb_2O_3 (2:2 in atomic ratio) was used as the source material. The temperature of the tube was increased to 700 °C at a speed of 10 deg min^{-1} with a flow of mixed gas (90% Ar, 10% O_2) at 180 sccm. The product in bulk form was obtained on the substrate mounted downward region of the furnace where the temperature was 100 °C less than that of the central regime.

* To whom correspondence should be addressed. E-mail: jzhu@mail.tsinghua.edu.cn. Fax: 86-10-62771160.
[†] Tsinghua University.
[‡] University of Science & Technology.

10.1021/jp100037u
Published on Web 01/25/2010

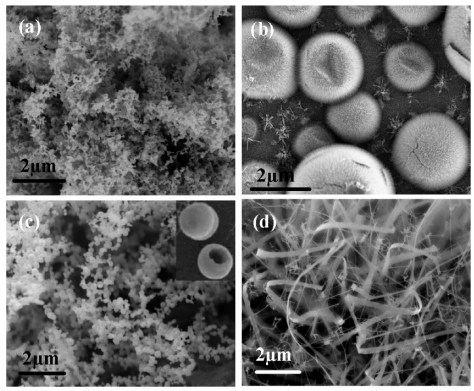

Figure 1. Field emission scanning electron microscopy images of (a) pure ZnO powder, (b) undoped ZnO microspheres composed of nanowires, (c) hollow Sb-doped ZnO nanospheres, and (d) Al-doped ZnO nanobelts.

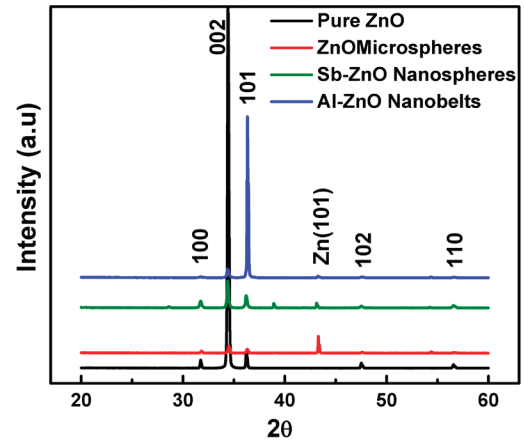

Figure 2. XRD pattern of the pure and as grown ZnO nanostructures.

3. Al-Doped ZnO Nanobelts. Al-doped ZnO nanobelts were synthesized by a simple one-step thermal process, where a bare cleaned Si substrate was used to obtain the synthetic product. Mixed powder Zn + Al_2O_3 (2:1 in atomic ratio) was used as the source material. The temperature of the tube was increased to 800 °C at a speed of 5 deg min^{-1} with a flow of mixed gas (80% Ar, 20% O_2) at 150 sccm. The substrate was mounted in the downward region of the furnace where the temperature was ~600 °C.

4. Apparatus. The as-prepared products were examined by a field emission scanning electron microscope (FESEM-6301F), a 800 °C high resolution transmission electron microscope (HRTEM-JEM2011), energy dispersive spectroscopy (EDS), and X-ray photospectroscopy (XPS). PL measurements were conducted at room temperature, using the 325 nm line of a He−Cd laser as the excitation source. The hydrogen storage properties including hydrogen absorption−desorption kinetics were measured by an isovolumetric method, using a PCT apparatus. This can be operated up to 10 MPa and at 600 °C. The pressure of hydrogen released in relation to volume was displayed by a pressure transducer. The experimental studies were done by a reactor that consisted of two parts: heater and sample vessel. The former was used to connect with the pressure transducer and thermocouple. The reactor had a 1.5 cm outer diameter (o.d.), 0.5 cm wall, and 20 cm internal length and it was loaded with the sample vessel (1 cm o.d., 0.1 cm wall, and 5 cm internal length). The reactor was heated with an air furnace. The mass of the sample used for testing was kept at 0.3 g for each and the temperature was controlled within ±1 K. From the magnitude of hydrogen pressure change, we could calculate the amount of the hydrogen absorbed and desorbed.

III. Results and Discussions

FESEM has been employed to analyze the morphology of the as-grown products. The morphology of the pure ZnO powder consists of nanoparticles as shown in Figure 1a. The morphology of undoped sample consists of hollow ZnO microspheres composed of vertically oriented straight NWs with a length in the range of micrometers as shown in Figure 1b. However, Sb-doped sample reveals that the product consists of hollow nanospheres as shown in Figure 1c. The diameter of nanospheres is in the range of ~50−400 nm. The morphology of the Al-doped sample consists of nanobelts with uniform diameter in the range of 30−200 nm and length in micrometers as shown in Figure 1d.

The structure and phase purity of the as-grown products has been characterized by using XRD as shown in Figure 2. All the major diffraction peaks in the patterns can be indexed to the pure ZnO wurtzite crystal structure. The presence of two weak Zn peaks in the pattern reveals that a small amount of Zn powder remains phase separated during the experiments. No separate phase of Sb and Al being identified confirms the successful substitution into the ZnO lattice. Furthermore, there are also some changes found in the intensity of diffraction peaks as compared with those of pure ZnO, which may be attributed to the crystalline quality of the nanostructures.

To further investigate the microstructure of prepared samples, the HRTEM and SAED measurements have been carried out over individual undoped and Sb- and Al-doped nanostructure, as shown in Figure 3a−i. The TEM and HRTEM image of ZnO NWs with diameters in the range of ~20−100 nm is shown in panels a and b of Figure 3, respectively. The corresponding selected area electron diffraction (SAED) shows the single crystalline wurtzite structure along [0001] as shown in the inset of Figure 3b. The EDS spectrum consists of an oxygen peak at about 0.52 keV, and Zn peaks at 1.02, 8.67, and 9.6 keV are shown in Figure 3c. The signals of Cu, C, and Cr peaks come from the copper grid used for TEM measurements. Figure 3d,e reveals the TEM and highly magnified image of Sb-doped ZnO nanospheres along with corresponding SAED (inset Figure 3e) and exhibits the polycrystalline nature of the nanospheres. The presence of Sb peaks in the EDS spectrum confirms the existence of Sb into nanospheres as shown in Figure 3f. The TEM and HRTEM image of the Al-doped ZnO nanobelt is shown in Figure 3g,h. The corresponding SAED pattern is found to be identical with the entire part of the nanobelt as shown in the inset of Figure 3h. The nanobelts are found to be single crystalline grown along the [0001] direction. The EDS for nanobelt confirms the incorporation of Al into nanobelts as shown in Figure 3i. Quantitative analysis reveals that the average amount of Al contents is about 2% in each of the nanobelts. Statistical analysis of EDS measurements over a dozen nanobelts demonstrates that the variation of Al contents is rather small and the composition of Al dopant is uniform throughout the specimen. Therefore, EDS results further demonstrate that Al is incorporated into ZnO, which is also in good agreement with the XRD results.

The valence state of the Sb and Al elements has been analyzed by XPS. Figure 4 shows the XPS survey along with Sb3d and Al2p peaks in the inset. The Sb-doped sample shows that the Sb peaks including O1s are located at 530 and 539.3 eV

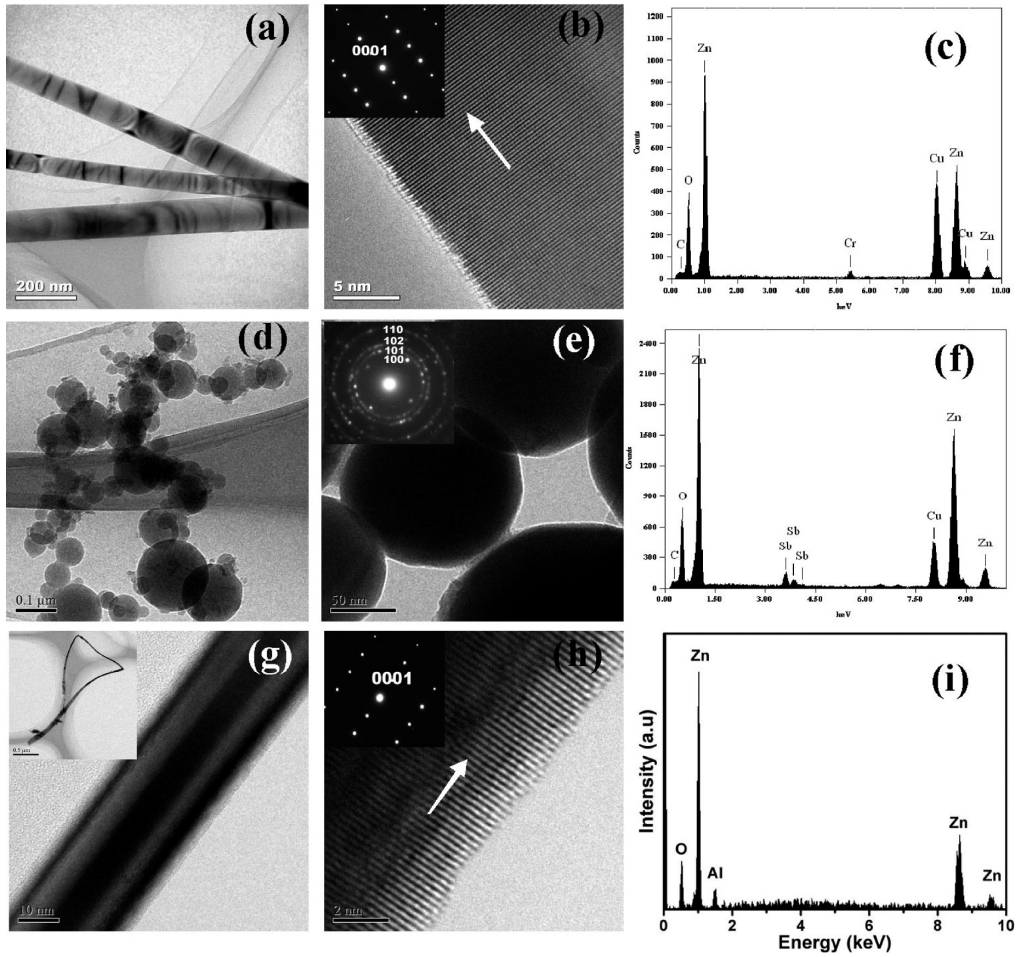

Figure 3. TEM, HRTEM images along with SAED (inset) and EDS of (a−c) ZnO microspheres composed of nanowires, (d−f) Sb-doped ZnO nanospheres, and (g−i) Al-doped ZnO nanobelts.

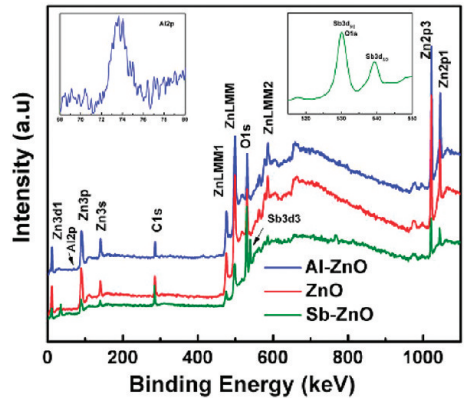

Figure 4. (a) XPS survey spectra of ZnO nanostructures. (inset: the XPS spectrum of the Sb-doped ZnO nanosphere corresponding to Sb3d5 and Sb3d3 peaks); XPS spectrum of Al-doped ZnO nanobelts corresponding to the Al2p peak.

corresponding to the electronic states of $Sb3d_{5/2}$ and $Sb3d_{3/2}$, respectively. The $Sb3d_{3/2}$ peak in the spectrum clearly indicates that the Sb element has been doped into nanospheres. However, the Al-doped sample shows that the Al peak is located at 73.8 eV corresponding to the electronic states of Al2p. The presence of Al peaks in the spectrum shows that Al is successfully substituted into the lattice. The XPS results are in good agreement with the previous reports in the literature.[20,21]

Figure 5a shows the room temperature PL spectra of as-prepared ZnO nanostructures excited by 325-nm UV light, using a He−Cd laser as a source. The PL spectra consist of a UV band peak at 377 nm and a broad green band centered at about 529 nm. The UV emission band could be related to a near band-edge (NBE) transition of ZnO, namely, the recombination of free excitons through an exciton collision process.[22] The green emission peak is commonly referred to as a deep-level or trap-state emission. The green band is generally explained by the radial recombination of a photogenerated hole with the electron in a singly ionized oxygen vacancy. It has been reported that due to the excess exciton impurity and crystalline defect scattering, there exists a deep-level emission at around 2.4 eV in the ZnO NWs.[23] The UV emission peak position of Sb and Al nanostructures exhibits a blue shift compared with that of pure ZnO. This may be attributed to the shift of the optical band gap induced by the introduction of impurities into ZnO nanostructures.[24,25] The intensity of the UV emission peak is suppressed in Al- and Sb-doped samples while the intensity of the visible band significantly increased due to increased oxygen vacancy defects as reported.[26] Up to now, many researchers have demonstrated that the defects play a very important role in the improvement of properties of materials.[27] On the basis of interesting PL results we focused our work on the study of hydrogen storage properties of nanostructures.

Hydrogen storage and release experiments of the nanostructures have been performed at 373 K. About 0.3 g of each nanostructure is employed and the hydrogen uptake experiments are performed under 5 MPa of pressure. After the nanostructures are installed in the storage chamber, they are heated at 400 °C for 30 min to remove impurities such as water and oxygen.

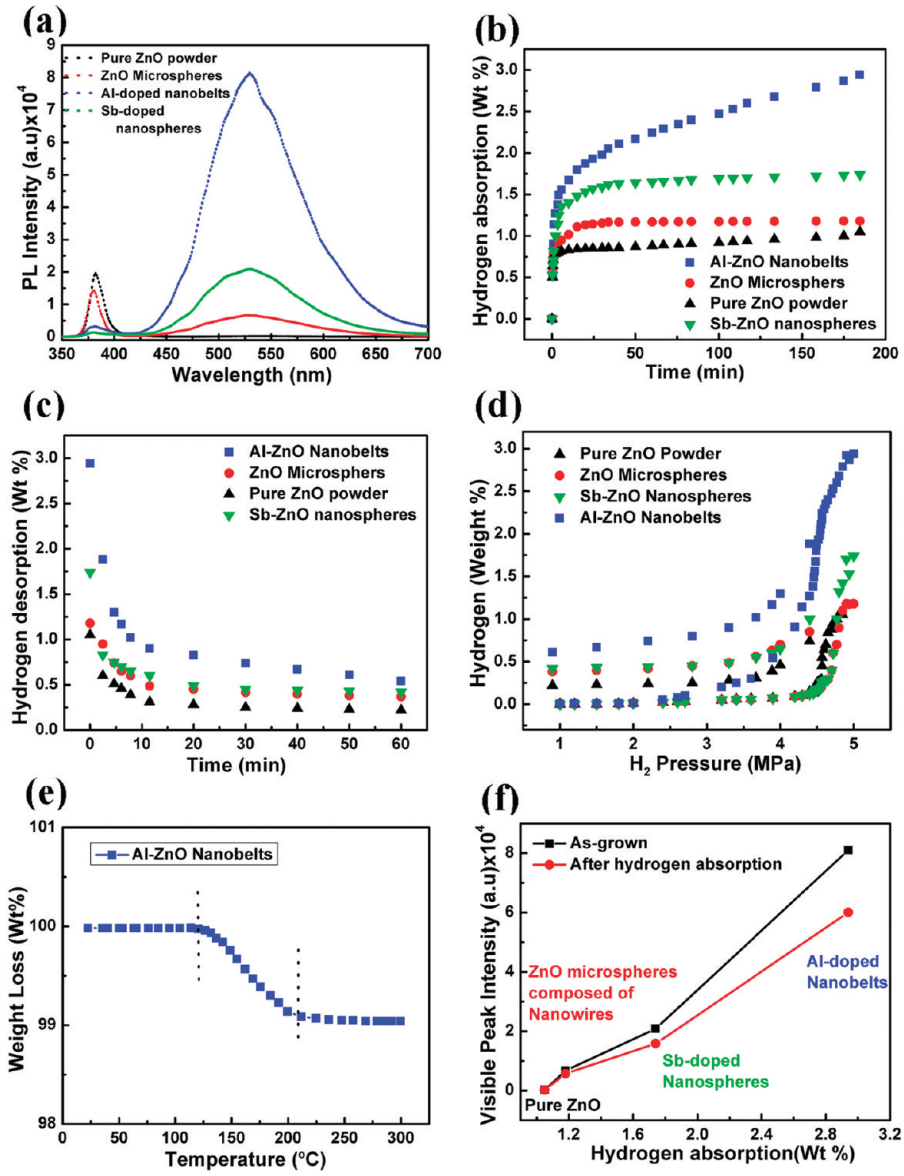

Figure 5. (a) Room temperature PL spectra of ZnO nanostructures; (b) hydrogen absorption kinetics curves at 373 K under an initial hydrogen pressure of 5.0 MPa for ZnO nanostructures; (c) hydrogen desorption kinetics curves at 373 K under an ambient pressure for ZnO nanostructures; (d) the pressure−composition isotherm of the four samples, i.e., ZnO powder, ZnO microspheres, Sb-doped ZnO nanospheres, and Al-doped ZnO nanobelts taken at 373 K; (e) TG analysis of the Al-doped ZnO nanobelts in the hydride state that was subjected to ambient pressure; and (f) relationship between hydrogen absorption and visible peak intensity before and after hydrogen absorption.

When the sample cell is cooled to 100 °C (~373 K), H_2 is admitted into the apparatus and the H_2 storage began. As shown in Figure 5b, after 3 h the hydrogen storage capacity of the commercial ZnO powder is found to be 1.05 wt %, ZnO microspheres 1.179 wt %, Sb-doped ZnO nanospheres 1.74 wt %, and Al-doped ZnO nanobelts about 2.94 wt %. It can be seen that hydrogen storage in Al-doped nanobelts gradually increases with the increase in time, which suggests that much more hydrogen can be stored into nanobelts. This fact can explain why the Al incorporation into nanobelts induces strong lattice defects (as clear from the PL spectra) which create interstitial sites for hydrogen atoms. The pressure of the reaction chamber is evacuated gradually to 1 atm (1.013105 Pa) for the hydrogen release process. As shown in Figure 5c about 79% of the stored hydrogen can be released under ambient pressure for commercial ZnO powder, 67% for ZnO microspheres, and 76% for Sb-doped ZnO nanospheres. We observe that the hydrogen release process is also very quick for Al-doped nanobelts, and 81.6% of the stored hydrogen can be released within 60 min. All these results illustrate that the presence of Al in ZnO nanobelts not only enhances the hydrogen storage capacity but also is considered a promising reversible hydrogen storage media.

Figure 5d shows the pressure composition isotherm of the four samples at 373 K. All samples (0.3 g) are evacuated and heated at 673 K for 2 h prior to the measurement. After the sample cell cools to 373 K, the hydrogen uptake experiments are performed for 3 h under a hydrogen pressure of 5 MPa. The absorption and desorption isotherm is stabilized after four cycles of measurements. The results shown in Figure 5d are those after the stabilization of the isotherm. From the results we can see that the plateaus are quite flat and broad and a small hysteresis gap between the absorption and desorption plateaus is observed, suggesting they have good hydrogen absorption and desorption reversibility. As can be seen from the curves, the PCIs of hydrogen absorption and desorption of Al-doped ZnO nanobelts exhibit longer plateaus due to taking up much more hydrogen than other samples under identical conditions.

TABLE 1: Comparison of Hydrogen Storage Characteristics of Some ZnO-Based Nanostructures

materials	absorption/wt %	pressure/MPa	temp/K	tested wt/g	ref
Al-ZnO nanobelts	2.94	5	373	0.3	present work
Sb-ZnO nanospheres	1.74	5	373	0.3	present work
ZnO microspheres	1.179	5	373	0.3	present work
pure ZnO	1.05	5	373	0.3	present work
ZnO NWs	0.83	3.03	300	0.3149	ref 18
Mg-ZnO NWs	2.79	5.93	300	0.5	ref 19

We can also see from the curves that the hydrogen storage capacity of the four samples starts at about 3 MPa and increases with the pressure up to 5 MPa.

The Al-doped ZnO nanobelt sample in the hydride state was subjected to ambient pressure for the thermogravimetry (TG) analysis as shown in Figure 5e. The TG analysis shows that desorption of hydrogen from 125 to 210 °C gives a total loss of about 1.0 wt % H_2. In fact the amount of hydrogen desorption in TG observation was detected at ambient pressure, illustrating that the weight loss was due to the portion of hydrogen remaining in the sample after the hydrogen environment was removed. This means that about 80% of the absorbed hydrogen at 5 MPa was already desorbed when lowering the hydrogen pressure to atmospheric conditions, but that 20% of the absorbed hydrogen was still retained, suggesting that this remaining hydrogen is chemisorbed.

The influence of hydrogen absorption on the optical properties of the nanostructures is also investigated by PL. Figure 5f shows the relation between hydrogen absorption and the visible (green emission) peak intensity before and after hydrogen absorption. It is found that hydrogen absorption has a direct corelation with the defects in the nanostructures. It is also seen that the hydrogen absorption significantly reduced the intensity of green emission, which is consistent with the previous reports that H_2 absorption has a passivation effect on the point defects or impurities, since the hydrogen atom can easily diffuse into the lattice and form strong bonds with various lattice positions. Ahn et al. report that oxygen vacancy defects in ZnO nanowire based gas sensors significantly enhance gas sensitivity.[28] Recently, Han et al. and Wan et al. report that hydrogen storage capacity is affected by the crystallinity of the nanostructures and larger amounts of oxygen vacancies are responsible for the high uptake capability [refs 18 and 19]. In our previous work we already reported that defects in tip shape ZnO NWs lead to a significant role in the sensing applications.[29] Our present results are in good agreement with the literature reports and show strong evidence for the corelation between defects and hydrogen storage capabilities of nanostructures. Hence, hydrogen absorption/desorption capability increased due to the oxygen vacancy defects in the nanostructures. Although there is a trend between oxygen vacancy defects and hydrogen absorption/desorption of four different nanostructures, a further study may be required to understand the precise mechanism of hydrogen storage in nanostructures.

The comparison of hydrogen storage characteristics of the present and previously reported ZnO-based nanostructures is also shown in the Table 1. It can be seen that among all nanostructures Al-doped nanobelts exhibit good hydrogen storage capacity and can be found useful for future nanotechnology. The improved hydrogen absorption/desorption behavior of Al-doped nanobelts may be due to the high surface-to-volume ratio. Furthermore, it has been reported that Al doping changse the acid−base characteristics of ZnO materials which also affects the gas-sensing characteristics of ZnO.

IV. Conclusions

In conclusion, hydrogen storage capabilities of ZnO-based nanostructures have been successfully investigated and found depending on doping elements. It is found that Al substitution into ZnO nanobelts has a catalytic effect on the hydrogen absorption and thus the kinetic properties are greatly enhanced. The improved hydrogen absorption/desorption behavior of Al-doped nanobelts may be due to the large specific surface area. Furthermore, an increase in the amount of oxygen vacancy defects due to dopants is found to be responsible for higher hydrogen uptake in nanostructures. In addition, it has been found that creating defects in nanostructures should make it possible to improve the hydrogen uptake capacity. To the best of our knowledge, this is the first time hydrogen storage capabilities of Al-doped and Sb-doped ZnO nanostructures have been studied. This study may provide a new platform for fuel cell design and play an important role for the applications in energy storage and high-energy batteries.

Acknowledgment. This work is financially supported by the National 973 Project of China and the Chinese National Nature Science Foundation. The authors also thank the Higher Education Commission (HEC) of Pakistan for the financial support to Mashkoor Ahmad.

References and Notes

(1) Lee, C. J.; Lee, T. J.; Lyu, S. C.; Zhang, Y.; Ruh, H.; Lee, H. J. *Appl. Phys. Lett.* **2002**, *81*, 3648.
(2) Kong, X.; Ding, Y.; Yang, R.; Wang, Z. L. *Science* **2004**, *303*, 1348.
(3) Liu, C. H.; Zapien, J. A.; Yao, Y.; Meng, X. M.; Lee, C. S.; Fan, S. S.; Lifshitz, Y.; Lee, S. T. *Adv. Mater.* **2003**, *15*, 838.
(4) Dell, R. M.; Rand, D. A. J. *J. Power Sources* **2001**, *100*, 2.
(5) Miller, J. F.; Chalk, S. G. *J. Power Sources* **2006**, *159*, 73.
(6) Sakintunaa, B.; Lamarri-Darkrimb, F.; Hirscherc, M. *Int. J. Hydrogen Energy* **2007**, *32*, 1121.
(7) Ahmad, M.; Zhao, J.; Iqbal, J.; Miao, W.; Xie, L.; Mo, R.; Zhu, J. *J. Phys. D: Appl. Phys.* **2009**, *42*, 165406.
(8) Zuttel, A.; Wenger, P.; Rentsch, S.; Sudan, P.; Mauron, Ph.; Emmenegger, Ch. *J. Power Sources* **2003**, *118*, 1.
(9) Gao, H.; Wu, X.; Li, J.; Wu, G.; Lin, J.; Wu, K.; Xu, D. *Appl. Phys. Lett.* **2003**, *83*, 3389.
(10) Grochala, W.; Edwards, P. P. *Chem. Rev.* **2004**, *104*, 1283.
(11) Vajo, J. J.; Skeith, S, L.; Mertens, F. *J. Phys. Chem. B* **2005**, *109*, 3719.
(12) Darkrim, F. L.; Malbrunot, P.; Tartaglia, G. P. *Int. J. Hydrogen Energy* **2002**, *27*, 193.
(13) Ma, R.; Bando, Y.; Zhu, H.; Sato, T.; Xu, C.; Wu, D. *J. Am. Chem. Soc.* **2002**, *124*, 7672.
(14) Chen, J.; Li, S. L.; Tao, Z. L.; Shen, Y. T.; Cui, C. X. *J. Am. Chem. Soc.* **2003**, *125*, 5284.
(15) Hui, P.; Yuan, P. F.; Jianyi, L. *Appl. Phys. Lett.* **2007**, *90*, 223104.
(16) Mpourmpakis, G.; Froudakis, G. E.; Lithoxoos, G. P.; Samio, J. *Nano Lett.* **2006**, *6*, 1581.
(17) Seayad, A. M.; Antonelli, D. V. *Adv. Mater.* **2004**, *16*, 765.
(18) Wan, Q.; Lin, C. L.; Yu, X. B.; Wang, T. H. *Appl. Phys. Lett.* **2004**, *84*, 124.
(19) Hui, P.; Jizhong, L.; Han, S.; Yuanping, F.; Cheekok, P.; Jianyi, L. *Nanotechnology* **2006**, *17*, 2963.
(20) Zeng, D. W.; Xie, C. S.; Zhu, B. L.; Song, W. L.; Wang, A. H. *Mater. Sci. Eng., B* **2003**, *104*, 68.

(21) Chang, S. Y.; Jung, S. K.; Jang, W. C.; Moo, H. K.; Young, J. K.; Jeong, G. C.; Geug, T. K. *J. Ind. Eng. Chem.* **2000**, *6*, 149.

(22) Kong, Y. C.; Yu, D. P.; Zhang, B.; Fang, W.; Feng, S. Q. *Appl. Phys. Lett.* **2001**, *78*, 407.

(23) Hu, J. Q.; Bando, Y. *Appl. Phys. Lett.* **2003**, *82*, 1401.

(24) Zhou, S. M.; Zhang, X. H.; Meng, X.; Zou, K.; Fan, X.; Wu, S.; Lee, S. T. *Nanotechnology* **2004**, *15*, 1152.

(25) Yang, P.; Yan, H.; Mao, S.; Russo, R.; Johnson, J.; Saykally, R.; Morris, N.; Phan, J.; He, R.; Choi, H. *Adv. Funct. Mater.* **2002**, *12*, 323.

(26) Bai, S. N.; Tsai, H. H.; Tseng, T. Y. *Thin Solid Films* **2007**, *516*, 155.

(27) Vanheusden, K.; Warren, W. L.; Seager, C. H.; Tallant, D. R.; Voigt, J. A.; Gnade, B. E. *J. Appl. Phys.* **1996**, *79*, 7983.

(28) Ahn, M. W.; Park, K. S.; Heo, J. H.; Park, J. G.; Kim, D. W.; Choi, K. J. I.; Lee, J. H.; Hong, S. H. *Appl. Phys. Lett.* **2008**, *93*, 263103.

(29) Ahmad, M.; Pan, C.; Iqbal, J.; Gan, L.; Zhu, J. *Chem. Phys. Lett.* **2009**, *480*, 105.

JP100037U